Applied Catalysis B: Environmental 334 (2023) 122847

Contents lists available at ScienceDirect

Applied Catalysis B: Environmental

journal homepage: www.elsevier.com/locate/apcatb

Rational design of D− π − A− π − D porous organic polymer with polarized π for photocatalytic aerobic oxidation

Kun Wu, Xin-Yi Liu, Mo Xie, Pei-Wen Cheng, Ji Zheng, Weigang Lu *, Dan Li *

College of Chemistry and Materials Science, and Guangdong Provincial Key Laboratory of Functional Supramolecular Coordination Materials and Applications, Jinan University, Guangzhou 510632, PR China

A R T I C L E I N F O

Keywords:
Porous organic polymer
Donor−π−acceptor−π−donor
Photocatalytic aerobic oxidation
Reactive oxygen species

A B S T R A C T

Charge separation and reactive oxygen species (ROS) generation efficiency are of foremost importance for photocatalytic aerobic oxidation reactions. In this study, four porous organic polymers (POPs), namely **JNU-208**, **-209**, **-210**, and **-211**, were designed and synthesized from linear bipyrazoles and cyanuric chloride through condensation reactions. The donor−acceptor−donor (D−A−D) type POP (**JNU-209**) exhibits improved photo-electrochemical properties relative to the donor–π–donor (D−π − D) type POP (**JNU-208**). Benzene and thiophene were further incorporated respectively as bridging π-units. The two corresponding D− π − A− π − D type POPs (**JNU-210** and **-211**) exhibit additionally enhanced photo-electrochemical properties. The four POPs were examined their potentials as photocatalysts for the aerobic oxidation of benzylamines, and **JNU-211** was found to have the highest photocatalytic activity. Theoretical calculations confirm that the introduction of thiophene not only increases the conjugation but also promotes the π-electron polarization, both of which facilitate charge separation and ROS generation.

1. Introduction

Over the past decades, visible-light-driven chemical transformations, in which solar energy is converted into chemical energy, have attracted growing interest in response to the goal of transitioning to green economy [1,2]. Among them, photocatalytic aerobic oxidation has become a hotspot in organic synthesis owing to their environmentally benign reaction conditions [3]. Ruthenium/iridium and other noble transition metal complexes are known for their photocatalytic activity and widely used as photocatalysts to date [4–6]. Yet, from the standpoint of green chemistry, the scarcity and non-recyclability of ruthenium/iridium complexes limit their large-scale applications. Thus, the development of inexpensive and recyclable heterogeneous photocatalysts could make a great contribution in the field of photocatalysis and further industrial applications. For example, many porous materials constructed with organic photosensitizers have been demonstrated not only good photocatalytic properties but also excellent recyclability [7–18]. However, more research efforts are needed to expand the visible-light absorption range and increase the charge separation efficiency of those heterogeneous noble-metal-free photocatalysts.

Porous organic polymers (POPs) are a class of covalently-linked purely-organic porous materials. They can achieve exceptionally high surface areas by judiciously selecting organic building blocks of different dimensions and geometries. Moreover, wet chemistry-based surface engineering can be applied to introduce diverse functions. POPs have been frequently explored in the fields of chemical sensing, gas adsorption/separation, and catalysis [19–29]. To date, using organic photosensitizers as building blocks to construct porous materials is one of the common strategies in the development of heterogeneous photocatalysts [30–33]. For example, by simultaneously incorporating donor (D) and acceptor (A) units into polymers, the resulting D−A type structures have been demonstrated to not only reduce the band gap but also extend the lifetime of the charge carriers [34–38]. In our previous work, we found that the D−A−D system may further improve the charge separation efficiency [10,11]. Meanwhile, the introduction of π units may increase the conjugation and electron delocalization, thereby expanding the visible-light response range and suppressing the charge carrier recombination [39,40]. For example, Zhang's group reported a g-C_3N_4-based polymer with benzene as a conjugated π unit, and the resulting copolymer (**UCN-BD**) showed wide visible-light absorption, controlled optical band gap, and good charge separation efficiency [40]. On the other hand, thiophene is often used as a π-spacer in catalysis, solar cells, and

* Corresponding authors.
E-mail addresses: weiganglu@jnu.edu.cn (W. Lu), danli@jnu.edu.cn (D. Li).

https://doi.org/10.1016/j.apcatb.2023.122847
Received 17 March 2023; Received in revised form 29 April 2023; Accepted 3 May 2023
Available online 4 May 2023

cancer therapy due to its high π–electron density and internal polarization [41–44]. For example, Zheng's group reported the synthesis of a covalent triazine framework (CTF) with a thiophene-containing linker, and the obtained **CTF-7** showed significantly improved charge separation efficiency [45]. Based on the above analysis, we envision the development of donor− π − acceptor− π − donor (D−π − A−π − D) type organic photosensitizers and their incorporation into porous materials may be able to further improve the charge separation efficiency in noble-metal-free photocatalysts.

Herein, we report the synthesis of four POPs (**JNU-208**, **-209**, **-210**, and **-211**, JNU = Jinan University) through condensation reactions between predesigned linear bipyrazoles and cyanuric chloride (Scheme 1). By tuning the conjugation and polarization of the bipyrazoles, the four POPs were found to gradually expand their visible-light absorption along with significantly different photo-electrochemical properties. Oxidative coupling of benzylamine was used as a model reaction to evaluate their photocatalytic performance. As expected, **JNU-211** exhibits the best photocatalytic activity with an almost quantitative yield (99%) in 12 h, substantially higher than **JNU-209** (76%), **JNU-210** (54%), and **JNU-208** (24%). Further experiments and theoretical calculations confirm that **JNU-211** possesses a more suitable band gap for ROS generation under visible-light irradiation. This work successfully demonstrates the rational design of D− π − A− π − D structures with polarized π-electron for improved photocatalytic aerobic oxidation performance.

2. Results and discussion

2.1. Structure and characterization

As depicted in Scheme 1, four POPs were obtained through condensation reactions between bipyrazoles and cyanuric chloride in the presence of *N,N*-diisopropylethylamine (DIPEA, see Supplementary Material for details, Fig. S1−S9) [46]. Take **JNU-211** as an example, approximately 50 mg of **JNU-211** was soaked in common solvents such as acetonitrile, ethanol, dichloromethane, ethyl acetate, acetone, dioxane, and H_2O for two days. Then, the supernatants were collected after centrifugation. As shown in Fig. S10, these supernatants are colorless liquids, in stark contrast to the bright red color of the organic precursor, indicating a substantial polymerization and good stability of **JNU-211** in these solvents. To further evaluate its practicality in photocatalytic reactions, the acetonitrile solution of **JNU-211** was heated up to 80 ℃ for 24 h. The color of supernatant remains unchanged, and no red-light emission was observed under UV light irradiation (λ = 365 nm), indicating that **JNU-211** is potentially recyclable as heterogeneous catalyst (Supplementary Fig. S11).

As shown in Fig. S12, powder X-ray diffraction (PXRD) patterns reveal all four POPs have a broad diffraction peak around $2\theta \approx 23^\circ$, suggesting the formation of graphitic-like stacked layer structures, consistent with the flake-like morphology as observed in the high-resolution transmission electron microscopy (HR-TEM) and scanning electron microscopy (SEM) images (Fig. 1c and 1d; Supplementary Fig. S13) [47,48]. Energy-dispersive X-ray spectroscopy (EDS) was performed to show that C, N, and S elements are well dispersed in the skeleton of **JNU-211** (Fig. 1e). To assess the porosity of these POP materials, the powder samples were heated up to 120 ℃ overnight before being subjected to N_2 adsorption/desorption measurements at 77 K (Fig. 1a and Supplementary Fig. S14). Brunauer-Emmett-Teller (BET) surface areas were determined to be 29 $m^2\ g^{-1}$, 48 $m^2\ g^{-1}$, 18 $m^2\ g^{-1}$, and 50 $m^2\ g^{-1}$ for **JNU-208**, **JNU-209**, **JNU-210**, and **JNU-211**, respectively. The pore size distribution of **JNU-211** was analyzed by HK method (Fig. 1a inset), showing the presence of micropores. Thermogravimetric analysis (TGA) was carried out on the as-prepared powder samples; the results indicate that all four POPs are stable up to 360 °C (Supplementary Fig. S15).

To confirm the successful construction of the polymeric structure, solid-state ^{13}C nuclear magnetic resonance (NMR) analysis of **JNU-211** was carried out. For comparisons, solution-state ^{13}C NMR analysis of its bipyrazole precursor (4,7-bis(5-(1 *H*-pyrazol-4-yl)thiophen-2-yl)benzo[*c*] [1,2,5]thiadiazole, BT-Th-Pz) and model compound (2,4,6-tris(4-(thiophen-2-yl)− 1*H*-pyrazol-1-yl)− 1,3,5-triazine, TTPT) were also carried out. As shown in Fig. 1b (iii), the signal at 163 ppm can be assigned to triazine carbons; the signal at 146 ppm to aromatic carbons adjacent to N atoms; the signals at 136, 133, 128, and 121 ppm to thiophene carbons; and the signals at 149, 131, and 118 ppm to benzothiadiazole carbons. The data are in good agreement with those of BT-Th-Pz and TTPT, indicating the structural integrity of **JNU-211**. All the Fourier-transform infrared (FT-IR) spectra of **JNU-208**−**211**

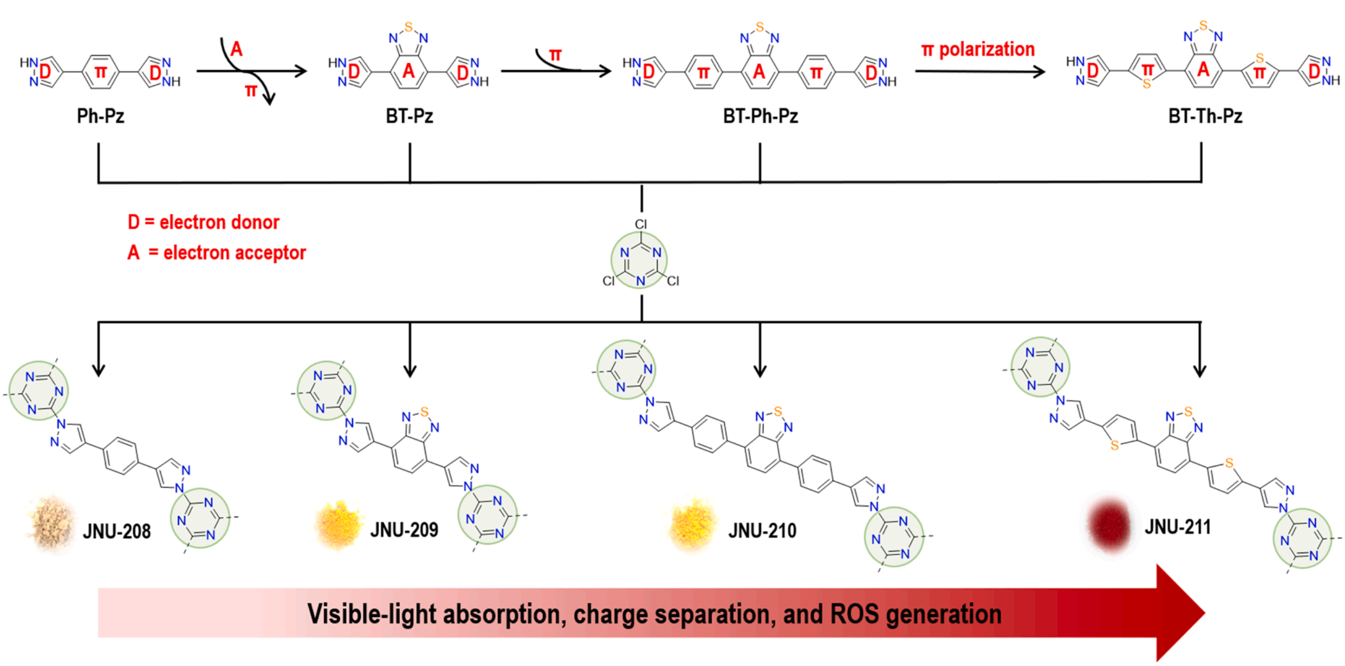

Scheme 1. Schematic illustration of designing D− π − A− π − D structures with polarized π-electron and their incorporation into POPs.

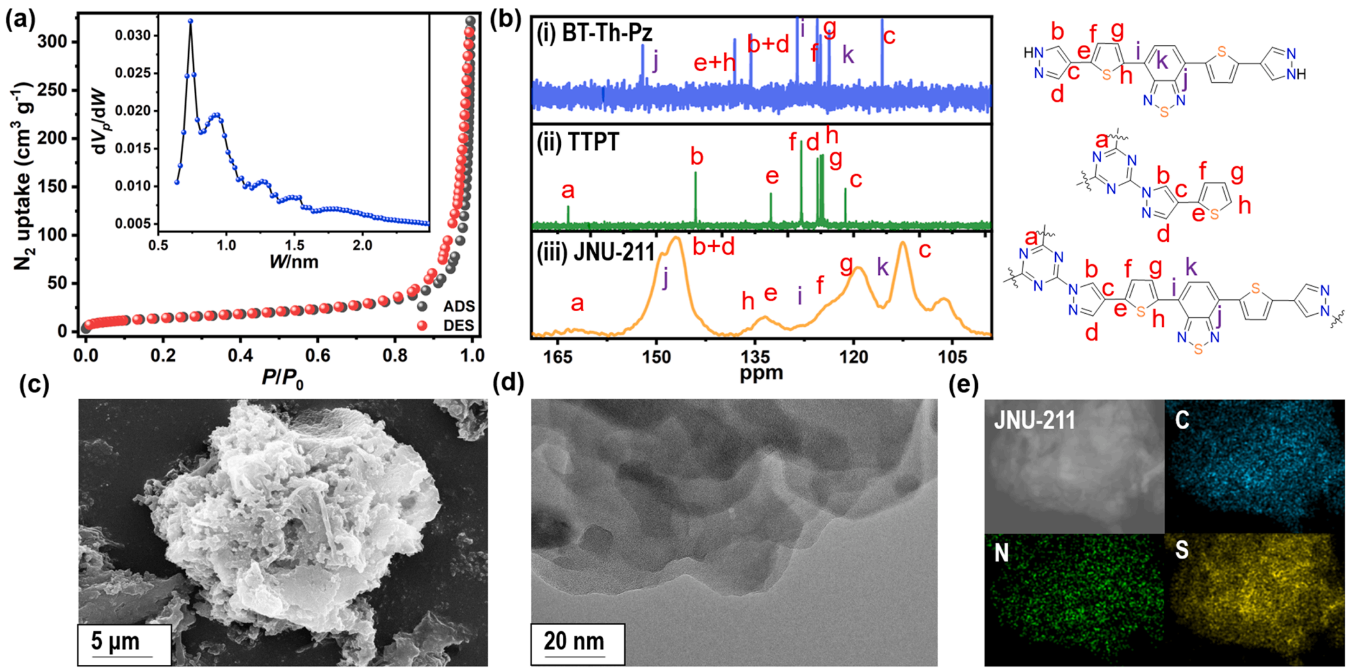

Fig. 1. (a) N_2 adsorption/desorption isotherms of **JNU-211** measured at 77 K (Inset: pore size distribution). (b) Solution-state ^{13}C NMR spectra of bipyrazole precursor BT-Th-Pz (i) and model compound TTPT (ii) as well as solid-state ^{13}C NMR spectrum of **JNU-211** (iii). (c) SEM image of the **JNU-211**. Scale bar = 5 μm. (d) HR-TEM image of **JNU-211**. Scale bar = 20 nm. (e) Elemental mapping (EDS) images of **JNU-211**.

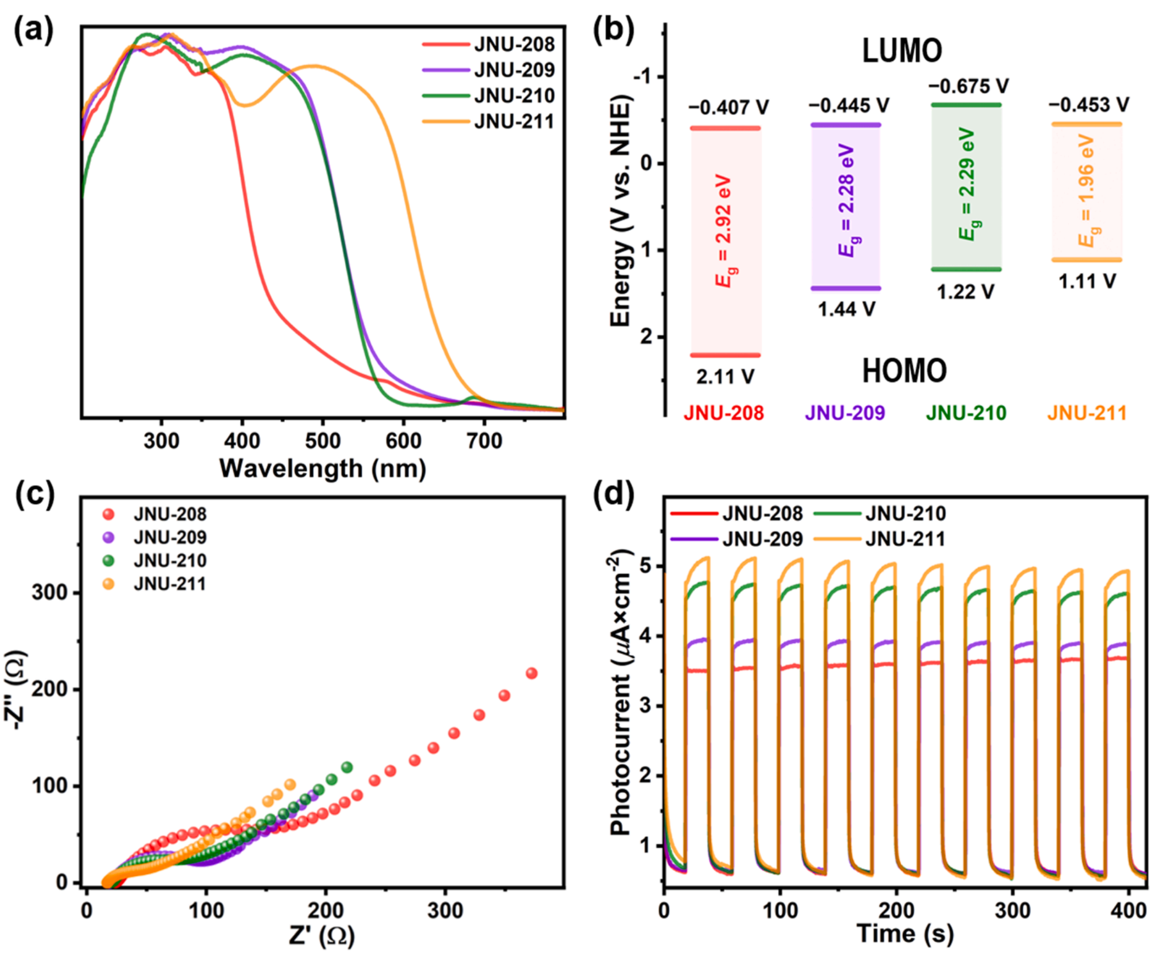

Fig. 2. (a) UV−visible diffuse reflectance spectra of **JNU-208 − 211**. (b) Schematic depiction of the optical band gaps of **JNU-208 − 211**. (c) EIS Nyquist plots for **JNU-208 − 211** in 0.50 M solution of Na_2SO_4. (d) Photocurrent response of **JNU-208 − 211** under visible light irradiation (λ = 420 −800 nm).

displayed new C−N stretching signals at around 1410 cm^{-1}, further confirming the successful preparation of these POPs (Supplementary Fig. S16).

The bonding states and elemental composition of **JNU-208−211** were analyzed by X-ray photoelectron spectroscopy (XPS). Take **JNU-211** as an example, the peaks at 284.28 eV and 285.18 eV on the XPS spectrum of C 1 s can be assigned to aromatic C−C and C−S bonds, respectively. The peak at 286.68 eV corresponds to C=N (triazine) [49–51]. The peak at 398.78 eV on the XPS spectrum of N 1 s belongs to C=N (triazine), and the broad peak at 400.13 eV can be attributed to the C=N in the benzothiadiazole and pyrazole units [46]. Furthermore, the peak at 165.58 eV on the XPS spectrum of S 2p can be assigned to S $2p_{1/2}$ (N − S), while the peaks at 164.58 eV (N − S) and 163.28 eV (C−S) can be assigned to S $2p_{3/2}$ (Supplementary Fig. S17−S20) [37,52].

2.2. Photochemistry and electrochemistry

The luminescence properties of the four bipyrazoles in *N,N*-dimethylformamide (DMF) were investigated with a 365 nm excitation at room temperature. As shown in Fig. S21−S24, The wavelength of the emission peak is in the order of BT-Th-Pz (693 nm) > BT-Ph-Pz (584 nm) ≈ BT-Pz (570 nm) > Ph-Pz (442 nm), which can be partially ascribed to the conjugation and polarization of π-spacers [53]. Specifically, the luminescence emission was red-shifted from 442 to 570 nm by replacing the benzene with benzothiadiazole (Ph-Pz to BT-Pz). Additionally, the further incorporation of benzene as π-spacer slightly red-shift the luminescence emission further to 584 nm (BT-Ph-Pz), whereas the incorporation of thiophene as π-spacer significantly red-shift the luminescence emission to 693 nm (BT-Th-Pz). On the other hand, the UV−visible diffuse reflectance spectra (UV−vis DRS) of the four POPs were measured, all of them showing slightly red-shifted luminescence emission compared to their corresponding bipyrazoles (Supplementary Fig. S25). Among them, **JNU-211** exhibits a visible-light absorption edge of ca. 700 nm due to the increased π-conjugation (Fig. 2a). Based on the Tauc plots (Supplementary Fig. S26), the optical band gaps were estimated to be ca. 2.92, 2.28, 2.29, and 1.96 eV for **JNU-208**, **JNU-209**, **JNU-210**, and **JNU-211**, respectively. The reduction of the band gap confirms that the introduction of thiadiazole and thiophene units can indeed improve the light-absorbing capacity. Further, the emission intensity of **JNU-211** is lower than those of the other POPs, indicating an enhanced charge separation in **JNU-211** due to π-electron polarization. **JNU-211** has a higher transient fluorescence lifetime (0.96 ns) compared to **JNU-208** (0.25 ns) and **JNU-210** (0.70 ns) (Supplementary Fig. S27), yet the luminescence lifetime of **JNU-211** is shorter than that of **JNU-209** (1.2 ns), probably due to the favorable nonradiative intersystem crossing pathway in **JNU-211**, suggesting the singlet excitons are more effectively converted to triplet excitons [54–57]. To further investigate the highest occupied molecular orbital (HOMO) and the lowest unoccupied molecular orbital (LUMO) levels, the Mott−Schottky plots of the four POPs were measured. From the onset of the Mott−Schottky curves, the LUMO levels were calculated to be − 0.607, − 0.645, − 0.875, and − 0.653 V *v.s.* Ag/AgCl (−0.407, −0.445, −0.675, and −0.453 V *v.s.* NHE) for **JNU-208**, **JNU-209**, **JNU-210**, and **JNU-211**, respectively (Supplementary Fig. S28) [58]. Their HOMO levels were thus determined to be 2.21 V, 1.44 V, 1.22 V, and 1.11 V *v.s.* NHE based on the equation of $E_g = E_{LUMO} - E_{HOMO}$ (Fig. 2b). Valence bond X-ray photoelectron spectroscopy (VB-XPS) measurements were performed (Fig. S29) and the HOMO positions of the four POPs were found consistent with the analysis from Mott−Schottky plots, further validating the accuracy of the band gap structures. Overall, these POPs have more negative potentials than that of $O_2/O_2^{\bullet-}$ couple (−0.33 V *v.s.* NHE), implying that all of them are capable of generating ROS [38,59].

The electrochemical impedance spectroscopy (EIS) measurements on the four POPs were carried out in 0.50 M Na_2SO_4 solution. As shown in Fig. 2c, the Nyquist plots for **JNU-210** and **JNU-211** show relatively smaller radii, suggesting that the POPs constructed with D− π − A− π − D units have higher charge migration ability and potentially faster charge separation in the photocatalytic process [58]. Furthermore, the transient photocurrent experiments show that the introduction of thiophene leads to a significant increase in the photocurrent density, implying favorable charge carrier transfer kinetics of **JNU-211** (Fig. 2d). Overall, optical and electrochemical studies suggest building the pyrazole−thiophene−benzothiadiazole−thiophene−pyrazole photosensitizer into the POP framework could substantially enhance the charge separation efficiency, which prompted us to investigate its catalytic properties as a heterogeneous photocatalyst.

2.3. Density functional theory (DFT) analysis

To further understand the contribution of thiophene as π-spacer, the dipole moments of BT-Pz, BT-Ph-Pz, and BT-Th-Pz were calculated by using density function theory (DFT) method, PBE0-D3(BJ)/6–311 G(d, p). As depicted in Fig. S30, BT-Th-Pz shows a dipole moment of 5.65 Debye, which is larger than those of BT-Ph-Pz (2.91 Debye) and BT-Pz (2.85 Debye), indicating that the introduction of thiophene improves the intermolecular polarity and enhances the in-plane charge transfer and redistribution [47,60,61]. Moreover, the HOMOs of Ph-Pz, BT-Pz, BT-Ph-Pz, and BT-Th-Pz are localized all over the molecules (Supplementary Fig. S31), while their LUMOs are primarily localized on the benzothiadiazole units and slightly extended into the π-spacers. These results confirm that benzothiadiazole acts as an electron acceptor, pyrazole as an electron donor, and benzene/thiophene as π-spacer. The calculated band gap energy shows that the one containing thiophene units is the smallest, further indicating that π-polarization is conducive to charge separation. In addition to charge separation efficiency, the O_2 adsorption potential is also one of the important factors that could greatly affect aerobic oxidation reactions [62]. As shown in Fig. 3 and Fig. S32, the binding energy of **JNU-211** for O_2 on the triazine unit is higher than those of the other three POPs. Moreover, thiadiazole and thiophene units exhibit stronger oxygen binding energy compared to benzene unit (Supplementary Fig. S33).

2.4. Reactive oxygen species generation

In general, superoxide anion radical ($O_2^{\bullet-}$) and singlet oxygen ($^1O_2$)

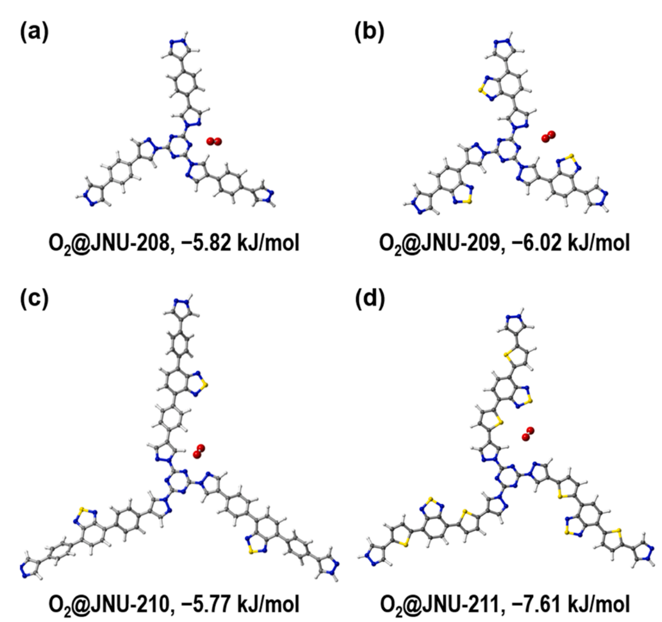

Fig. 3. Oxygen binding energies of **JNU-208**, **JNU-209**, **JNU-210** and **JNU-211** on triazine units.

are the dominant reactive oxygen species (ROS) in the photocatalytic aerobic oxidation reactions, therefore, we evaluated the $O_2^{\bullet -}$ generation efficiency of the four POPs by using nitro blue tetrazolium (NBT) [63, 64]. As shown in Fig. 4a, the UV-Vis absorption of NBT at 259 nm was decreased in the presence of all four POPs under visible-light irradiation, and the ratio of $O_2^{\bullet -}$ generation rates was estimated to be 1/1.19/1.42/2.63 for **JNU-208/JNU-209/JNU-210/JNU-211**. Likewise, 1,5-dihydroxynaphthalene (DHN) was used for probing the $^1O_2$ generation [65]. The efficiency of $^1O_2$ generation can be evaluated by the peak intensity at 298 nm on the UV-Vis absorption spectra of DHN (Fig. 4b), and the ratio of $^1O_2$ generation rates was estimated to be 1/9.99/16.94/19.45 for **JNU-208/JNU-209/JNU-210/JNU-211**. From the above results, we are confident that the introduction of thiophene and benzothiadiazole groups renders **JNU-211** with the most efficient $O_2^{\bullet -}$ and $^1O_2$ generation under visible-light irradiation. Electron paramagnetic resonance (EPR) measurements were further carried out to confirm the ROS generation by **JNU-211**. When 2,2,6,6-tetramethylpiperidine (TEMP) was used as a scavenger for $^1O_2$, three characteristic peaks of the radical TEMP$-^1O_2$ compounds were observed, and the intensity of the peaks was enhanced with prolonged irradiation time (Fig. 4c). When 5,5-dimethyl-1-pyrroline *N*-oxide (DMPO) was used as an indicator for $O_2^{\bullet -}$, six characteristic peaks of the radical DMPO$-O_2^{\bullet -}$ compounds were observed, and the intensity of the peaks was enhanced with prolonged irradiation time (Fig. 4d).

2.5. Photocatalytic aerobic oxidation of benzylamines

Encouraged by the excellent photoelectronic properties of **JNU-211**, we decided to assess its photocatalytic performance in the aerobic oxidation of benzylamines under visible-light irradiation. As shown in Table 1 (entry 1), the oxidative coupling of benzylamine can be achieved in 99% yield with **JNU-211** (4.0 mg) as photocatalyst, significantly higher than those with **JNU-210** (54%), **JNU-209** (76%), and **JNU-208** (24%) (entries 15 −17). Interestingly, **JNU-210**, the one with non-polarized π-electron (benzene), was less effective than **JNU-209**, the one without π-electron, further emphasizing the importance of π-electron polarization. Control experiments (entries 2 −5) show almost no reaction in the absence of **JNU-211**, light source, or air, indicating the indispensability of these reaction parameters. A similar yield was obtained when ambient air was replaced by pure O_2 (entry 6). The change of reaction solvent can significantly affect the photocatalytic efficiency, with acetonitrile being the highest (CH_3CN) in terms of yield (entries 1 and 7 −9). The yield was decreased from 99% to 88% when the loading of **JNU-211** was reduced from 4.0 to 2.0 mg (entries 10).

To verify the rationality of designing D− π − A− π − D structures for photocatalysis, all four bipyrazole molecules were evaluated as photocatalysts for the same reaction under similar conditions, the results indicate that the π-polarized D− π − A− π − D molecule can indeed afford the highest yield (entries 11 −14 and Table S2), confirming the importance of π-electron polarization in enhancing the photocatalytic efficiency of benzylamine oxidation [66]. Moreover, benzylamine

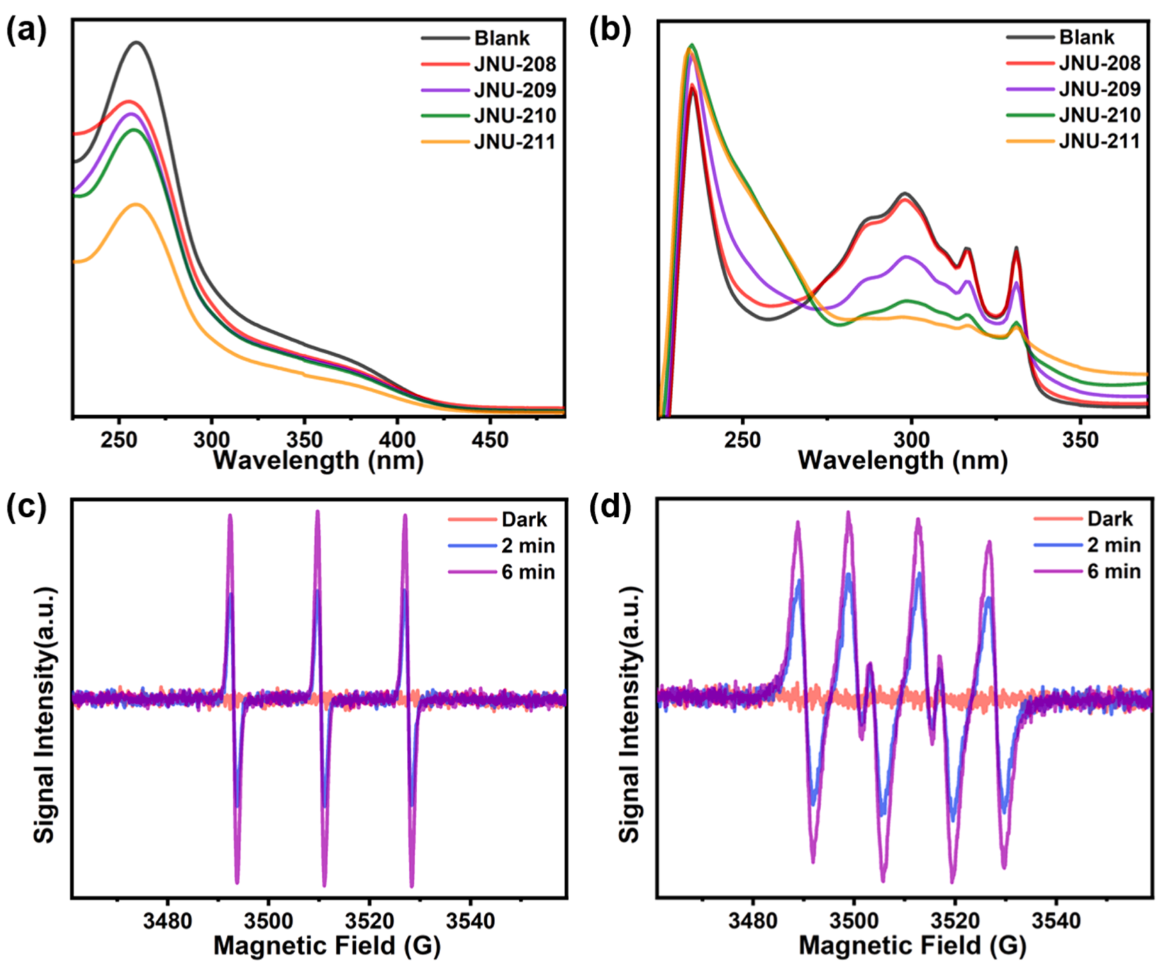

Fig. 4. (a) UV−vis absorption spectra of NBT (blank), NBT + **JNU-208**, NBT + **JNU-209**, NBT + **JNU-210**, and NBT + **JNU-211** upon visible light irradiation for 15 min; (b) UV−vis absorption spectra of DHN (blank), DHN + **JNU-208**, DHN + **JNU-209**, DHN + **JNU-210**, and DHN + **JNU-211** upon visible light irradiation for 6 min; (c) EPR spectra of **JNU-211** in the presence of TEMP under dark condition or visible-light irradiation (λ = 400 −470 nm); (d) EPR spectra of **JNU-211** in the presence of DMPO under dark condition or visible-light irradiation.

Table 1
Photocatalytic oxidative coupling of benzylamine[a].

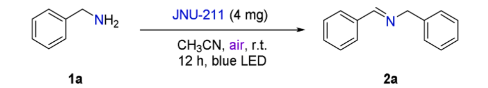

entry	change from the "standard conditions"	yield (%)[b]
1	none	99
2	no **JNU-211**	26
3	no hν	3
4	no hν, 80 °C	4
5	under N_2, instead of air	28
6	under O_2, instead of air	99
7	CH_2Cl_2, instead of CH_3CN	65
8	THF, instead of CH_3CN	74
9	CH_3OH, instead of CH_3CN	12
10	2 mg **JNU-211**	88
11	Ph-Pz (4 mg), instead of **JNU-211**	12
12	BT-Pz (4 mg), instead of **JNU-211**	68
13	BT-Ph-Pz (4 mg), instead of **JNU-211**	63
14	BT-Th-Pz (4 mg), instead of **JNU-211**	72
15	**JNU-208** (4 mg), instead of **JNU-211**	24
16	**JNU-209** (4 mg), instead of **JNU-211**	76
17	**JNU-210** (4 mg), instead of **JNU-211**	54

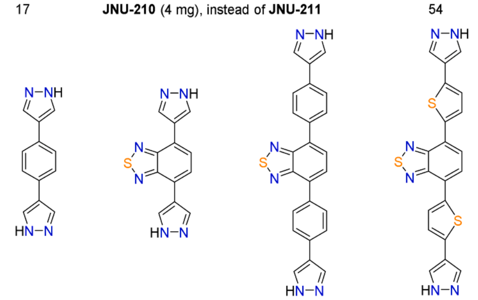
Ph-Pz BT-Pz BT-Ph-Pz BT-Th-Pz

[a]Reaction conditions: **1a** (0.50 mmol), **JNU-211** (4.0 mg), CH_3CN (4.0 mL), r.t., 12 h, blue LED, under air atmosphere. [b]H NMR yield with 1,1,2,2-tetrachloroethane ($C_2H_2Cl_4$) as the internal standard.

derivatives with different substituents were used instead under the optimized reaction conditions to examine the generality of **JNU-211** as a photocatalyst (Table 2). Moderate to good yields were obtained for benzylamines with either electron donating groups such as −Me, −OMe, − *n*-Bu, and −Et, or electron withdrawing groups such as −F, −Cl, −Br, and $-CF_3$ (**2b**−**2k**). In addition, the yield was barely affected by the substitution position of the methyl group (**2b**, **2j**, and **2k**). It is worth noting that the reaction can also work on 4-pyridinemethanamine with a moderate yield (**2i**, 56%).

2.6. Photocatalytic reaction mechanisms

Based on the above experimental results and previous reports, a plausible mechanism for this photocatalytic aerobic oxidation reaction was proposed (Fig. 5) [58,67–71]. We first performed two control experiments to study the ROS involved in this reaction. As seen in Fig. S34 and S35, by using NaN_3 (5.0 equiv.) as $^1O_2$ scavenger, the yield was decreased to 49%. While by adding *p*-benzoquinone (BQ, 5.0 equiv.) as $O_2^{\bullet-}$ scavenger, the formation of the target product was not detected. These results suggest that $O_2^{\bullet-}$ could be playing a more crucial role than $^1O_2$ in this oxidative coupling reaction [72]. As depicted in Fig. 5, $O_2^{\bullet-}$ and $^1O_2$ were generated via singlet electron transfer (SET) and energy transfer (ET) processes, respectively. The generated $^1O_2$ abstracts two hydrogen atoms from benzylamine to form the imine intermediate PhCH=NH, which was coupled with another benzylamine to generate the target product **2a** by releasing an ammonia molecule. The generated $O_2^{\bullet-}$, on the other hand, transforms the amine radical cation **A** into a labile iminium cation **B**, which was coupled with another benzylamine molecule to form intermediate **C**, and then, the target product **2a** by releasing an ammonia molecule. Notably, the formation of H_2O_2 was detected by using iodimetry method during the reactions (Supplementary Fig. S36) [73].

Table 2
Photocatalytic oxidative coupling of benzylamine derivatives [a,b].

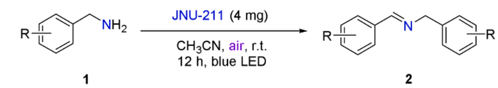

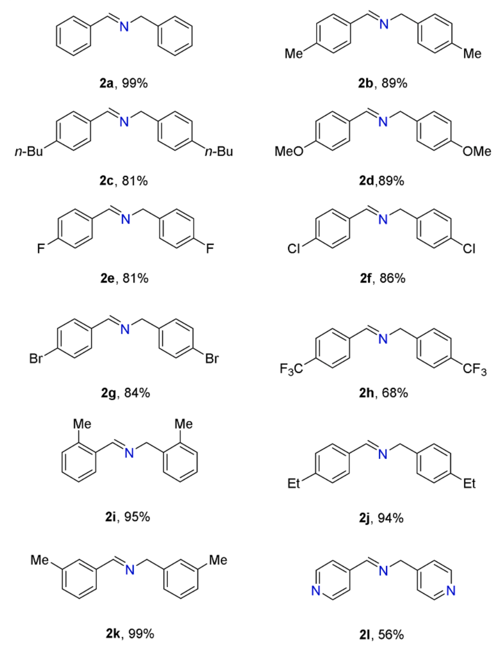

[a]Reaction conditions: **1a** (0.50 mmol), **JNU-211** (4.0 mg), CH_3CN (4.0 mL), r.t., 12 h, blue LED, under air atmosphere. [b]H NMR yield with 1,1,2,2-tetrachloroethane ($C_2H_2Cl_4$) as the internal standard.

2.7. Recyclability tests

To evaluate the feasibility of **JNU-211** as heterogeneous photocatalyst, recycling experiments were conducted for the benzylamine oxidation reactions and the yields were barely changed for four cycles (Supplementary Fig. S37). Furthermore, the FT-IR spectra, SEM images, and XPS spectra of **JNU-211** before and after photocatalysis show no obvious differences, suggesting the retention of the framework integrity (Supplementary Fig. S38−S40).

3. Conclusions

In summary, four POPs were designed and synthesized by using D− π − D, D−A−D, D− π − A− π − D, and π-polarized D− π − A− π − D type bipyraozle precursors through condensation reactions with cyanuric chloride. The π-polarized D− π − A− π − D system endows the corresponding POP (**JNU-211**) with the best photoelectrochemical properties, which was reflected in the photocatalytic aerobic oxidation of benzylamines. This work not only successfully illustrates the vital role of the π-polarized D− π − A− π − D system in the enhancement of photocatalytic performance but also provides a rational strategy of designing noble-metal-free photocatalysts for strong visible-light absorption, fast charge separation, and high ROS generation efficiency.

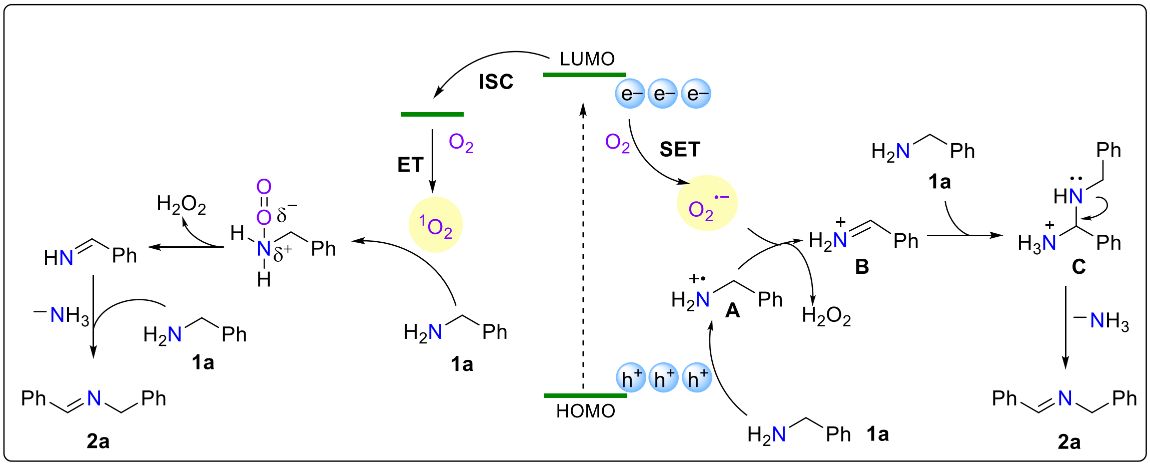

Fig. 5. Proposed reaction mechanism for the photocatalytic aerobic oxidation of benzylamine in the presence of **JNU-211**.

CRediT authorship contribution statement

Kun Wu: Investigation, Formal analysis, Data curation, Writing – original draft; **Xin-Yi Liu**: Investigation, Formal analysis; **Mo Xie**: Software, Visualization; **Pei-Wen Cheng**: Investigation, Formal analysis; **Ji Zheng**: Visualization; **Weigang Lu**: Conceptualization, Supervision, Writing – review & editing and Funding acquisition; **Dan Li**: Conceptualization, Supervision, Writing – review & editing and Funding acquisition.

Declaration of Competing Interest

The authors declare that they have no known competing financial interests or personal relationships that could have appeared to influence the work reported in this paper.

Data availability

Data will be made available on request.

Acknowledgements

This work was financially supported by the National Natural Science Foundation of China (Nos. 21731002, 21975104, 22101099, 22150004, and 22271120), the Guangdong Major Project of Basic and Applied Research (2019B030302009), and the Outstanding Innovative Talents Cultivation Funded Programs for Doctoral Students of Jinan University (No. 2022CXB007).

Appendix A. Supporting information

Supplementary data associated with this article can be found in the online version at doi:10.1016/j.apcatb.2023.122847.

References

[1] N.A. Romero, D.A. Nicewicz, Organic photoredox catalysis, Chem. Rev. 116 (2016) 10075–10166, https://doi.org/10.1021/acs.chemrev.6b00057.
[2] E. Romero, J.R. Gomez Castellanos, G. Gadda, M.W. Fraaije, A. Mattevi, Same substrate, many reactions: oxygen activation in flavoenzymes, Chem. Rev. 118 (2018) 1742–1769, https://doi.org/10.1021/acs.chemrev.7b00650.
[3] Z. Guo, B. Liu, Q. Zhang, W. Deng, Y. Wang, Y. Yang, Recent advances in heterogeneous selective oxidation catalysis for sustainable chemistry, Chem. Soc. Rev. 43 (2014) 3480–3524, https://doi.org/10.1039/c3cs60282f.
[4] L. Shi, W. Xia, Photoredox functionalization of C-H bonds adjacent to a nitrogen atom, Chem. Soc. Rev. 41 (2012) 7687–7697, https://doi.org/10.1039/c2cs35203f.
[5] D.M. Schultz, T.P. Yoon, Solar synthesis: prospects in visible light photocatalysis, Science 343 (2014) 1239176, https://doi.org/10.1126/science.1239176.
[6] C.K. Prier, D.A. Rankic, D.W. MacMillan, Visible light photoredox catalysis with transition metal complexes: applications in organic synthesis, Chem. Rev. 113 (2013) 5322–5363, https://doi.org/10.1021/cr300503r.
[7] Z. Wang, X. Hu, Z. Liu, G. Zou, G. Wang, K. Zhang, Recent developments in polymeric carbon nitride-derived photocatalysts and electrocatalysts for nitrogen fixation, ACS Catal. 9 (2019) 10260–10278, https://doi.org/10.1021/acscatal.9b03015.
[8] J. Luo, X. Zhang, J. Zhang, Carbazolic porous organic framework as an efficient, metal-free visible-light photocatalyst for organic synthesis, ACS Catal. 5 (2015) 2250–2254, https://doi.org/10.1021/acscatal.5b00025.
[9] R. Li, J. Byun, W. Huang, C. Ayed, L. Wang, K.A.I. Zhang, Poly(benzothiadiazoles) and their derivatives as heterogeneous photocatalysts for visible-light-driven chemical transformations, ACS Catal. 8 (2018) 4735–4750, https://doi.org/10.1021/acscatal.8b00407.
[10] K. Wu, J.-K. Jin, X.-Y. Liu, Y.-L. Huang, P.-W. Cheng, M. Xie, J. Zheng, W. Lu, D. Li, Thiadiazole-functionalized metal–organic frameworks for photocatalytic C–N and C–C coupling reactions: tuning the ROS generation efficiency via cobalt introduction, J. Mater. Chem. C. 10 (2022) 11967–11974, https://doi.org/10.1039/d2tc02559k.
[11] J.K. Jin, K. Wu, X.Y. Liu, G.Q. Huang, Y.L. Huang, D. Luo, M. Xie, Y. Zhao, W. Lu, X. P. Zhou, J. He, D. Li, Building a pyrazole-benzothiadiazole-pyrazole photosensitizer into metal-organic frameworks for photocatalytic aerobic oxidation, J. Am. Chem. Soc. 143 (2021) 21340–21349, https://doi.org/10.1021/jacs.1c10008.
[12] Z.H. Long, D. Luo, K. Wu, Z.Y. Chen, M.M. Wu, X.P. Zhou, D. Li, Superoxide ion and singlet oxygen photogenerated by metalloporphyrin-based metal-organic frameworks for highly efficient and selective photooxidation of a sulfur mustard simulant, ACS Appl. Mater. Inter. 13 (2021) 37102–37110, https://doi.org/10.1021/acsami.1c08840.
[13] H. Huang, X.-S. Wang, D. Philo, F. Ichihara, H. Song, Y. Li, D. Li, T. Qiu, S. Wang, J. Ye, Toward visible-light-assisted photocatalytic nitrogen fixation: a titanium metal organic framework with functionalized ligands, Appl. Catal. B: Environ. 267 (2020), 118686, https://doi.org/10.1016/j.apcatb.2020.118686.
[14] X. Ren, F. Liu, Q. Wang, H. Song, S. Luo, S. Li, G. Yang, B. Deng, Z. Huang, X.-S. Wang, L. Shi, J. Ye, Engineering interfacial charge transfer channel for efficient photocatalytic H_2 evolution: The interplay of CoPx and Ca^{2+} dopant, Appl. Catal. B: Environ. 303 (2022), 120887, https://doi.org/10.1016/j.apcatb.2021.120887.
[15] N. Hu, Y. Cai, L. Li, X. Wang, J. Gao, Amino-functionalized titanium based metal-organic framework for photocatalytic hydrogen production, Molecules 27 (2022) 4241, https://doi.org/10.3390/molecules27134241.
[16] A. Zhang, P. Dong, Y. Wang, K. Gao, J. Pan, B. Yang, X. Xi, J. Zhang, Fabrication of well-dispersed Pt nanoparticles onto the donor-acceptor type conjugated polymers for high-efficient photocatalytic hydrogen evolution, Appl. Catal. A: Gen. 644 (2022), https://doi.org/10.1016/j.apcata.2022.118793.
[17] P. Dong, A. Zhang, J. Pan, K. Gao, Z. Wang, X. Xi, An all-organic S-scheme heterojunction containing donor–acceptor type conjugated polymer and C_3N_4 nanosheets assembled via π–π interaction for photocatalytic H_2 generation, Appl. Surf. Sci. 615 (2023), https://doi.org/10.1016/j.apsusc.2023.156414.
[18] P. Dong, A. Zhang, T. Cheng, J. Pan, J. Song, L. Zhang, R. Guan, X. Xi, J. Zhang, 2D/2D S-scheme heterojunction with a covalent organic framework and g-C_3N_4 nanosheets for highly efficient photocatalytic H_2 evolution, Chinese, J. Catal. 43 (2022) 2592–2605, https://doi.org/10.1016/s1872-2067(22)64094-4.
[19] R.K. Totten, Y.S. Kim, M.H. Weston, O.K. Farha, J.T. Hupp, S.T. Nguyen, Enhanced catalytic activity through the tuning of micropore environment and supercritical CO_2 processing: Al(porphyrin)-based porous organic polymers for the degradation of a nerve agent simulant, J. Am. Chem. Soc. 135 (2013) 11720–11723, https://doi.org/10.1021/ja405495u.
[20] W. Wang, A. Zheng, P. Zhao, C. Xia, F. Li, Au-NHC@Porous organic polymers: synthetic control and its catalytic application in alkyne hydration reactions, ACS Catal. 4 (2013) 321–327, https://doi.org/10.1021/cs400983y.

[21] L. Li, H. Zhao, R. Wang, Tailorable synthesis of porous organic polymers decorating ultrafine palladium nanoparticles for hydrogenation of olefins, ACS Catal. 5 (2015) 948–955, https://doi.org/10.1021/cs501731w.

[22] Q. Sun, Z. Dai, X. Liu, N. Sheng, F. Deng, X. Meng, F.S. Xiao, Highly efficient heterogeneous hydroformylation over Rh-metalated porous organic polymers: synergistic effect of high ligand concentration and flexible framework, J. Am. Chem. Soc. 137 (2015) 5204–5209, https://doi.org/10.1021/jacs.5b02122.

[23] R. Li, Z.J. Wang, L. Wang, B.C. Ma, S. Ghasimi, H. Lu, K. Landfester, K.A.I. Zhang, Photocatalytic selective bromination of electron-rich aromatic compounds using microporous organic polymers with visible light, ACS Catal. 6 (2016) 1113–1121, https://doi.org/10.1021/acscatal.5b02490.

[24] J. Luo, X. Zhang, J. Lu, J. Zhang, Fine tuning the redox potentials of carbazolic porous organic frameworks for visible-light photoredox catalytic degradation of lignin β-O-4 Models, ACS Catal. 7 (2017) 5062–5070, https://doi.org/10.1021/acscatal.7b01010.

[25] K. Huang, J.-Y. Zhang, F. Liu, S. Dai, Synthesis of porous polymeric catalysts for the conversion of carbon dioxide, ACS Catal. 8 (2018) 9079–9102, https://doi.org/10.1021/acscatal.8b02151.

[26] S. Kramer, N.R. Bennedsen, S. Kegnæs, Porous organic polymers containing active metal centers as catalysts for synthetic organic chemistry, ACS Catal. 8 (2018) 6961–6982, https://doi.org/10.1021/acscatal.8b01167.

[27] A. Atilgan, M.M. Cetin, J. Yu, Y. Beldjoudi, J. Liu, C.L. Stern, F.M. Cetin, T. Islamoglu, O.K. Farha, P. Deria, J.F. Stoddart, J.T. Hupp, Post-synthetically elaborated BODIPY-based porous organic polymers (POPs) for the photochemical detoxification of a sulfur mustard simulant, J. Am. Chem. Soc. 142 (2020) 18554–18564, https://doi.org/10.1021/jacs.0c07784.

[28] X. Li, X. Ma, F. Zhang, X. Dong, X. Lang, Selective photocatalytic formation of sulfoxides by aerobic oxidation of sulfides over conjugated microporous polymers with thiazolo[5,4-*d*]thiazole linkage, Appl. Catal. B: Environ. 298 (2021), 120514, https://doi.org/10.1016/j.apcatb.2021.120514.

[29] Y. Liu, J. Wu, F. Wang, Dibenzothiophene-S,S-dioxide-containing conjugated polymer with hydrogen evolution rate up to 147 mmol g^{-1} h^{-1}, Appl. Catal. B: Environ. 307 (2022), https://doi.org/10.1016/j.apcatb.2022.121144.

[30] Q. Liao, W. Xu, X. Huang, C. Ke, Q. Zhang, K. Xi, J. Xie, Donor-acceptor type [4+3] covalent organic frameworks: sub-stoichiometric synthesis and photocatalytic application, Sci. China Chem. 63 (2020) 707–714, https://doi.org/10.1007/s11426-019-9696-3.

[31] J.A. Johnson, J. Luo, X. Zhang, Y.-S. Chen, M.D. Morton, E. Echeverría, F.E. Torres, J. Zhang, Porphyrin-metalation-mediated tuning of photoredox catalytic properties in metal–organic frameworks, ACS Catal. 5 (2015) 5283–5291, https://doi.org/10.1021/acscatal.5b00941.

[32] C. Lin, X. Liu, B. Yu, C. Han, L. Gong, C. Wang, Y. Gao, Y. Bian, J. Jiang, Rational modification of two-dimensional donor-acceptor covalent organic frameworks for enhanced visible light photocatalytic activity, ACS Appl. Mater. Inter. 13 (2021) 27041–27048, https://doi.org/10.1021/acsami.1c04880.

[33] S. Goswami, C.E. Miller, J.L. Logsdon, C.T. Buru, Y.L. Wu, D.N. Bowman, T. Islamoglu, A.M. Asiri, C.J. Cramer, M.R. Wasielewski, J.T. Hupp, O.K. Farha, Atomistic approach toward selective photocatalytic oxidation of a mustard-gas simulant: a case study with heavy-chalcogen-containing PCN-57 analogues, ACS Appl. Mater. Inter. 9 (2017) 19535–19540, https://doi.org/10.1021/acsami.7b07055.

[34] Y. Jiang, H. Liu, X. Li, Y. Yuan, J. Wang, B. Cui, Y. Li, Alkyloxime-substituted thiophene-based wide-band-gap polymer donor achieving a high short circuit current density of 30 mA cm^{-2} in organic solar cells, Chem. Mater. 34 (2022) 4232–4241, https://doi.org/10.1021/acs.chemmater.2c00929.

[35] J.T. Blaskovits, M. Fumanal, S. Vela, R. Fabregat, C. Corminboeuf, Identifying the trade-off between intramolecular singlet fission requirements in donor–acceptor copolymers, Chem. Mater. 33 (2021) 2567–2575, https://doi.org/10.1021/acs.chemmater.1c00057.

[36] S. Ma, T. Deng, Z. Li, Z. Zhang, J. Jia, G. Wu, H. Xia, S.W. Yang, X. Liu, Photocatalytic hydrogen production on a sp^2-carbon-linked covalent organic framework, Angew. Chem. Int. Ed. 61 (2022), e202208919, https://doi.org/10.1002/anie.202208919.

[37] C. Li, D. Li, W. Zhang, H. Li, G. Yu, Towards high-performance resistive switching behavior through embedding a D-A system into 2D imine-linked covalent organic frameworks, Angew. Chem. Int. Ed. 60 (2021) 27135–27143, https://doi.org/10.1002/anie.202112924.

[38] G. Li, W. Tian, C. Zhong, Y. Yang, Z. Lin, Construction of donor-acceptor heteroporous covalent organic frameworks as photoregulated oxidase-like nanozymes for sensing signal amplification, ACS Appl. Mater. Inter. 14 (2022) 21750–21757, https://doi.org/10.1021/acsami.2c04391.

[39] X. Li, F. Zhang, Y. Wang, K. Xiong, X. Lang, Extending the 2D conjugated microporous polymers linked by thiazolo[5,4-*d*]thiazole for green light-driven selective aerobic oxidation of amines, J. Mater. Chem. A 10 (2022) 14965–14975, https://doi.org/10.1039/d2ta02603a.

[40] K. Li, W.D. Zhang, Creating graphitic carbon nitride based donor-π-acceptor-π-donor structured catalysts for highly photocatalytic hydrogen evolution, Small 14 (2018), e1703599, https://doi.org/10.1002/smll.201703599.

[41] M.E. Cinar, T. Ozturk, Thienothiophenes, dithienothiophenes, and thienoacenes: syntheses, oligomers, polymers, and properties, Chem. Rev. 115 (2015) 3036–3140, https://doi.org/10.1021/cr500271a.

[42] Z. Sun, Y. Jiang, L. Zeng, L. Huang, Intramolecular charge transfer and extended conjugate effects in donor-π-acceptor-type mesoporous carbon nitride for photocatalytic hydrogen evolution, ChemSusChem 12 (2019) 1325–1333, https://doi.org/10.1002/cssc.201802890.

[43] L. Teng, G. Song, Y. Liu, X. Han, Z. Li, Y. Wang, S. Huan, X.B. Zhang, W. Tan, Nitric oxide-activated "dual-key-one-lock" nanoprobe for in vivo molecular imaging and high-specificity cancer therapy, J. Am. Chem. Soc. 141 (2019) 13572–13581, https://doi.org/10.1021/jacs.9b05901.

[44] L. Li, W.-y Lo, Z. Cai, N. Zhang, L. Yu, Donor–acceptor porous conjugated polymers for photocatalytic hydrogen production: the importance of acceptor comonomer, Macromolecules 49 (2016) 6903–6909, https://doi.org/10.1021/acs.macromol.6b01764.

[45] M. Liu, K. Jiang, X. Ding, S. Wang, C. Zhang, J. Liu, Z. Zhan, G. Cheng, B. Li, H. Chen, S. Jin, B. Tan, Controlling monomer feeding rate to achieve highly crystalline covalent triazine frameworks, Adv. Mater. 31 (2019), e1807865, https://doi.org/10.1002/adma.201807865.

[46] J. Yu, X. Sun, X. Xu, C. Zhang, X. He, Donor-acceptor type triazine-based conjugated porous polymer for visible-light-driven photocatalytic hydrogen evolution, Appl. Catal. B: Environ. 257 (2019), 117935, https://doi.org/10.1016/j.apcatb.2019.117935.

[47] C. Wu, Z. Teng, C. Yang, F. Chen, H.B. Yang, L. Wang, H. Xu, B. Liu, G. Zheng, Q. Han, Polarization engineering of covalent triazine frameworks for highly efficient photosynthesis of hydrogen peroxide from molecular oxygen and water, Adv. Mater. 34 (2022), e2110266, https://doi.org/10.1002/adma.202110266.

[48] C.T.J. Ferguson, N. Huber, K. Landfester, K.A.I. Zhang, Dual-responsive photocatalytic polymer nanogels, Angew. Chem. Int. Ed. 58 (2019) 10567–10571, https://doi.org/10.1002/anie.201903309.

[49] L. Fan, R. Ma, Y. Yang, S. Chen, B. Lu, Covalent sulfur for advanced room temperature sodium-sulfur batteries, Nano Energy 28 (2016) 304–310, https://doi.org/10.1016/j.nanoen.2016.08.056.

[50] F. Yu, L. Wang, Q. Xing, D. Wang, X. Jiang, G. Li, A. Zheng, F. Ai, J.-P. Zou, Functional groups to modify *g*-C_3N_4 for improved photocatalytic activity of hydrogen evolution from water splitting, Chin. Chem. Lett. 31 (2020) 1648–1653, https://doi.org/10.1016/j.cclet.2019.08.020.

[51] H. Ye, N. Gong, Y. Cao, X. Fan, X. Song, H. Li, C. Wang, Y. Mei, Y. Zhu, Insights into the role of protonation in covalent triazine framework-based photocatalytic hydrogen evolution, Chem. Mater. 34 (2022) 1481–1490, https://doi.org/10.1021/acs.chemmater.1c02697.

[52] S. Li, L. Dai, L. Li, A. Dong, J. Li, X. Meng, B. Wang, P. Li, Post-oxidation of a fully conjugated benzotrithiophene-based COF for photocatalytic detoxification of a sulfur mustard simulant, J. Mater. Chem. A 10 (2022) 13325–13332, https://doi.org/10.1039/d2ta01864k.

[53] B. Wu, Y. Liu, Y. Zhang, L. Fan, Q.-Y. Li, Z. Yu, X. Zhao, Y.-C. Zheng, X.-J. Wang, Molecular engineering of covalent triazine frameworks for highly enhanced photocatalytic aerobic oxidation of sulfides, J. Mater. Chem. A 10 (2022) 12489–12496, https://doi.org/10.1039/d2ta01441f.

[54] W. Zhang, Z. Deng, J. Deng, C.-T. Au, Y. Liao, H. Yang, Q. Liu, Regulating the exciton binding energy of covalent triazine frameworks for enhancing photocatalysis, J. Mater. Chem. A 10 (2022) 22419–22427, https://doi.org/10.1039/d2ta06479k.

[55] X.Y. Huang, Y.L. Lu, G.J. Mao, S.H. Yin, B. Long, G.J. Deng, A. Ali, T. Song, Polarization engineering of porous organic polymers for superior photocatalytic synthesis of disulfides and CO_2 reduction, J. Mater. Chem. A 10 (2022) 24147–24155, https://doi.org/10.1039/d2ta06941e.

[56] D. Chen, W. Chen, G. Zhang, S. Li, W. Chen, G. Xing, L. Chen, N-rich 2D heptazine covalent organic frameworks as efficient metal-free photocatalysts, ACS Catal. 12 (2021) 616–623, https://doi.org/10.1021/acscatal.1c05233.

[57] H. Wang, S. Jiang, S. Chen, D. Li, X. Zhang, W. Shao, X. Sun, J. Xie, Z. Zhao, Q. Zhang, Y. Tian, Y. Xie, Enhanced singlet oxygen generation in oxidized graphitic carbon nitride for organic synthesis, Adv. Mater. 28 (2016) 6940–6945, https://doi.org/10.1002/adma.201601413.

[58] H. Liu, C. Xu, D. Li, H.L. Jiang, Photocatalytic hydrogen production coupled with selective benzylamine oxidation over MOF composites, Angew. Chem. Int. Ed. 57 (2018) 5379–5383, https://doi.org/10.1002/anie.201800320.

[59] Y. Nosaka, A.Y. Nosaka, Generation and detection of reactive oxygen species in photocatalysis, Chem. Rev. 117 (2017) 11302–11336, https://doi.org/10.1021/acs.chemrev.7b00161.

[60] W. Gao, M. Zhang, T. Liu, R. Ming, Q. An, K. Wu, D. Xie, Z. Luo, C. Zhong, F. Liu, F. Zhang, H. Yan, C. Yang, Asymmetrical ladder-type donor-induced polar small molecule acceptor to promote fill factors approaching 77% for high-performance nonfullerene polymer solar cells, Adv. Mater. 30 (2018), e1800052, https://doi.org/10.1002/adma.201800052.

[61] Z. You, B. Wang, Z. Zhao, Q. Zhang, W. Song, C. Zhang, X. Long, Y. Xia, Metal-Free carbon-Based covalent organic frameworks with heteroatom-Free units boost efficient oxygen reduction, Adv. Mater. 35 (2023) 2209129, https://doi.org/10.1002/adma.202209129.

[62] Q. Niu, Q. Huang, T.Y. Yu, J. Liu, J.W. Shi, L.Z. Dong, S.L. Li, Y.Q. Lan, Achieving high photo/thermocatalytic product selectivity and conversion via thorium clusters with switchable functional ligands, J. Am. Chem. Soc. 144 (2022) 18586–18594, https://doi.org/10.1021/jacs.2c08258.

[63] H. Ben, G. Yan, H. Liu, C. Ling, Y. Fan, X. Zhang, Local spatial polarization induced efficient charge separation of squaraine-linked COF for enhanced photocatalytic performance, Adv. Funct. Mater. 32 (2021) 2104519, https://doi.org/10.1002/adfm.202104519.

[64] Y. Guo, H. Wen, T. Zhong, H. Huang, Z. Lin, Edge-rich atomic-layered BiOBr quantum dots for photocatalytic molecular oxygen activation, Chem. Eng. J. 445 (2022), 136776, https://doi.org/10.1016/j.cej.2022.136776.

[65] Z.W. Jiang, Y.C. Zou, T.T. Zhao, S.J. Zhen, Y.F. Li, C.Z. Huang, Controllable synthesis of porphyrin-based 2D lanthanide metal-organic frameworks with

thickness- and metal-node-dependent photocatalytic performance, Angew. Chem. Int. Ed. 59 (2020) 3300–3306, https://doi.org/10.1002/anie.201913748.
[66] J. Yu, S. Chang, X. Xu, X. He, C. Zhang, Photocatalytic hydrogen evolution based on nitrogen-containing donor–acceptor (D–A) organic conjugated small molecules, ACS Sustain. Chem. Eng. 8 (2020) 14253–14261, https://doi.org/10.1021/acssuschemeng.0c05964.
[67] Y. Zhang, J. Pang, J. Li, X. Yang, M. Feng, P. Cai, H.C. Zhou, Visible-light harvesting pyrene-based MOFs as efficient ROS generators, Chem. Sci. 10 (2019) 8455–8460, https://doi.org/10.1039/c9sc03080h.
[68] F.J. Zhao, G. Zhang, Z. Ju, Y.X. Tan, D. Yuan, The combination of charge and energy transfer processes in MOFs for efficient photocatalytic oxidative coupling of amines, Inorg. Chem. 59 (2020) 3297–3303, https://doi.org/10.1021/acs.inorgchem.9b03743.
[69] C. Xu, H. Liu, D. Li, J.H. Su, H.L. Jiang, Direct evidence of charge separation in a metal-organic framework: efficient and selective photocatalytic oxidative coupling of amines via charge and energy transfer, Chem. Sci. 9 (2018) 3152–3158, https://doi.org/10.1039/c7sc05296k.
[70] F. Zhang, J. Ma, Y. Tan, G. Yu, H. Qin, L. Zheng, H. Liu, R. Li, Construction of porphyrin porous organic cage as a support for single cobalt atoms for photocatalytic oxidation in visible light, ACS Catal. 12 (2022) 5827–5833, https://doi.org/10.1021/acscatal.2c00625.
[71] X. Dong, F. Zhang, F. Huang, X. Lang, Pyrene-based conjugated microporous polymers for red light-powered oxidation of amines to imines, Appl. Catal. B: Environ. 318 (2022), 121875, https://doi.org/10.1016/j.apcatb.2022.121875.
[72] F. Zhang, X. Li, X. Dong, H. Hao, X. Lang, Thiazolo[5,4-*d*]thiazole-based covalent organic framework microspheres for blue light photocatalytic selective oxidation of amines with O_2, Chinese, J. Catal. 43 (2022) 2395–2404, https://doi.org/10.1016/s1872-2067(22)64127-5.
[73] X. Liu, R. Qi, S. Li, W. Liu, Y. Yu, J. Wang, S. Wu, K. Ding, Y. Yu, Triazine-porphyrin-based hyperconjugated covalent organic framework for high-performance photocatalysis, J. Am. Chem. Soc. 144 (2022) 23396–23404, https://doi.org/10.1021/jacs.2c09369.